Stability of Lithium Hydride in Argon and Air

Ruiming Ren,[†,‡] Angel L. Ortiz,[§] Tippawan Markmaitree,[†] William Osborn,[†] and Leon L. Shaw*[,†]

Department of Materials Science and Engineering, University of Connecticut, Storrs, CT 06269-3136, School of Materials Science and Engineering, Dalian Jiaotong University, Dalian, China, and Departamento de Electrónica e Ingeniería Electromecánica, Universidad de Extremadura, Badajoz, Spain.

Received: January 4, 2006; In Final Form: April 7, 2006

The oxidation behaviors of LiH under a high purity argon atmosphere, an argon atmosphere with some O_2 and H_2O impurities, and ambient air at both room and high temperatures, are investigated using a variety of analytical instruments including X-ray diffractometry, thermogravimetry, mass spectrometry, scanning electron microscopy, and specific surface area analysis. The oxidation behaviors of the ball-milled LiH under different atmospheres are also studied and compared with those without ball milling. It is shown that no oxidation of LiH occurs under a high-purity argon atmosphere. However, oxidation of LiH takes place when the argon atmosphere contains some H_2O and O_2 impurities. At temperatures higher than ~55 °C, oxidation of LiH proceeds via the reaction of $LiH + {}^1/_4\ O_2 = {}^1/_2\ Li_2O + {}^1/_2\ H_2$, whereas at room temperature oxidation of LiH is likely caused by the simultaneous reactions of $LiH + H_2O = LiOH + H_2$ and $LiH + {}^1/_2\ O_2 = LiOH$. The oxidation behavior of LiH in ambient air with a 27% relative humidity can be well described by the Johnson−Mehl−Avrami equation. Furthermore, the ball-milled LiH oxidizes faster than the unmilled one, which is due to the finer particle size and larger surface area of the ball-milled powder.

I. Introduction

Li_3N-based materials have recently been investigated for their potential as hydrogen storage materials.[1−10] It is generally agreed that the hydrogen storage in Li_3N takes place in two steps, as shown in equations 1 and 2, with a total gravimetric density of 10.4 wt % H_2 and volumetric density of ~140 kg H_2/m^3.[1,6,7,11]

$$Li_3N + H_2 = Li_2NH + LiH \quad (1)$$

$$Li_2NH + H_2 = LiNH_2 + LiH \quad (2)$$

Lithium hydride (LiH) is present in both steps, and plays a critical role in preventing the formation of ammonia (NH_3).[4,5] It has been shown that the reverse process of eq 2, i.e., dehydriding of the lithium amide ($LiNH_2$) and lithium hydride mixture, proceeds with two elementary reactions, as defined by equations 3 and 4.[4,5]

$$LiNH_2 = {}^1/_2\ Li_2NH + {}^1/_2\ NH_3 \quad (3)$$

$${}^1/_2\ NH_3 + {}^1/_2\ LiH = {}^1/_2\ LiNH_2 + {}^1/_2\ H_2 \quad (4)$$

As shown in eqs 3 and 4, one complete cycle of these two elementary successive reactions consumes 50% $LiNH_2$ and 50% LiH in the powder mixture. Such successive reactions would continue until all $LiNH_2$ and LiH completely transform to Li_2NH and H_2. Reaction 4 takes place extremely fast, on the order of microseconds.[4] As such, escaping of NH_3 from the hydrogen storage system is prevented. However, if LiH is oxidized, the oxidation product(s) would no longer capture NH_3, and escaping of NH_3 occurs.[4]

Because of the unique role played by LiH in the hydrogen storage reactions of Li_3N-based materials, the stability of LiH under a high-purity argon atmosphere, an argon atmosphere containing some O_2 and H_2O impurities, and ambient air, would be of interest from both scientific and technological viewpoints. The understanding of such stability would shed light on how to handle and store LiH powder in order to prevent its oxidation. It may also provide a base to understand the cyclic stability of Li_3N-based materials in hydrogen uptake and release cycles. This becomes especially important if impurities enter the hydrogen storage tank with each refueling.

The reaction of LiH with water vapor has been investigated quite extensively.[12−15] It is established that when the amount of water is only sufficient to react with one surface layer of LiH, Li_2O forms via the following reaction[13]

$$LiH + {}^1/_2\ H_2O = {}^1/_2\ Li_2O + H_2 \quad (5)$$

However, when the amount of water is sufficient to react with several surface layers of LiH, LiOH forms via the following reaction[13]

$$LiH + H_2O = LiOH + H_2 \quad (6)$$

At even higher moisture levels, the formation of $LiOH{\cdot}H_2O$ is observed.[13−15]

The stability of LiH in an environment with the co-presence of O_2 and H_2O, on the other hand, is less investigated.[14] This is especially true for LiH under an argon atmosphere containing trace amounts of O_2 and H_2O simultaneously. With this in mind, this study investigates the oxidation behavior of LiH under a

* Corresponding author. Phone: 1 (860) 486-2592. Fax: 1 (860) 486-4745. E-mail: leon.shaw@uconn.edu.

† Department of Materials Science and Engineering, University of Connecticut.

‡ School of Materials Science and Engineering, Dalian Jiaotong University.

§ Departamento de Electrónica e Ingeniería Electromecánica, Universidad de Extremadura.

10.1021/jp060068m CCC: $33.50 © 2006 American Chemical Society
Published on Web 05/09/2006

high purity argon atmosphere, an argon atmosphere with some O_2 and H_2 impurities, and ambient air at both room and high temperatures. Comparisons in the oxidation behavior among these different environments are performed. Furthermore, since ball milling is widely used to enhance the kinetics of hydrogen uptake and release of hydrogen storage materials,[16−20] the oxidation behaviors of the ball-milled LiH under these different atmospheres are also investigated and compared with those without ball milling.

II. Experimental Section

Lithium hydride with 95% purity was purchased from Sigma-Aldrich. High-energy ball milling was performed using a modified Szegvari attritor that has been shown to be effective in preventing the formation of the dead zone and producing uniform milling products within the powder charge.[21] The canister of the attritor and balls 6.4 mm in diameter were both made of stainless steel. The loading of balls and the powder to the canister was performed in a glovebox filled with ultrahigh purity argon that contains Ar 99.999%, $H_2O < 1$ ppm, $O_2 < 1$ ppm, $H_2 < 3$ ppm, $N_2 < 5$ ppm, and THC < 0.5 ppm (to be referred to as Ar of 99.999% purity hereafter). The ball-to-powder weight ratio was 60:1, the milling speed was 600 rpm, and the milling temperature was maintained at 20 °C, achieved by water cooling at a flowing rate of 770 mL/min. The high-energy ball milling for all the samples studied lasted for 3 h.

All the samples before and after high-energy ball milling were subjected to various characterizations and handled in a glovebox filled with Ar of 99.999% purity. The specific surface area (SSA) of the LiH powders before and after high-energy ball milling were determined through nitrogen adsorption at 77 K based on the Brunauer−Emmett−Teller (BET) method[22] using a gas sorption analyzer (NOVA 1000). The loading of the LiH sample (~0.40 g) into a sample cell with a Teflon stem filler was performed in a glovebox filled with Ar of 99.999% purity. The measurement was performed immediately after the sample was loaded in the instrument without a degassing treatment. The relative pressure (P/P_o) was 0.05−0.3 and the reported SSA data were calculated based on 5 points BET method.

The oxidation behavior of LiH in ambient air was evaluated by installing LiH powders with and without ball milling individually in an X-ray diffractometer holder and exposing the powders to ambient air directly at room temperature. X-ray diffraction (XRD) patterns of the interested powder as a function of the exposing time were collected from the same sample repetitively in a pre-designed time interval. The operation conditions for the XRD data collection were CuK_α radiation, 40 kV, 40mA, 5°/min, and 0.02°/step using a D8 ADVANCE diffractometer. Before being installed in the XRD holder, some LiH samples were mixed with pure silicon powder. Since silicon is stable in air at room-temperature, the position of Si peaks can provide a baseline for a quick correction of the instrumental aberrations in the XRD patterns, and is thus useful for a better phase identification and lattice parameter determination in the oxidized LiH powder. A dehumidifier was installed next to the XRD instrument in order to maintain a constant relative humidity of ambient air during the XRD data collection. The relative humidity was constantly monitored and all the data were collected with 25−30% relative humidity.

Two types of experiments were performed to quantify the oxidation behavior of LiH under an argon atmosphere. The first was the thermogravimetric analysis (TGA) which was conducted using a TA instrument (TGA Q500). LiH samples of 25−55 mg were loaded into a Pt-microbalance pan with a short exposure to air (less than 30 s). The system was then flushed immediately with Ar of 99.999% purity for 90 min before heating from 20 to 600 °C with a heating rate of 5 °C/min. The argon flow rate was maintained at 60 mL/min in the entire holding and heating process. The outlet gas from TGA was constantly analyzed using a quadrupole residual gas analyzer (RGA) equipped with a mass spectrometer (model ppt-c300-F2Y). The gases monitored included H_2, N_2, O_2, H_2O, and Ar. To quantify the composition of the outlet gas, the RGA was calibrated using two calibration gases, with one containing 21.71 vol % H_2 and 78.29 vol % Ar and the other 301 ppm N_2, 1210 ppm O_2, 1990 ppm NH_3, and balance Ar. Furthermore, the detection limits of the RGA, determined using a flowing Ar of 99.999% purity, were 47, 49, 20, and 916 ppm for H_2, N_2, O_2, and H_2O, respectively.

The second set of experiments to quantify the oxidation behavior of LiH under an argon atmosphere was X-ray diffraction analysis of various types of LiH powders held inside a sealed capillary tube which helped to prevent oxidation of LiH powder during the XRD data collection. The loading of the powder to the capillary tube was performed in a glovebox filled with Ar of 99.999% purity. The capillary quartz tube had a wall of 0.01 mm thick and thus was transparent to the X-ray. Four types of LiH powders were studied in this set of experiments. They included (i) the as-purchased LiH powder, (ii) the ball-milled powder, (iii) the powder with ball milling and subsequently being stored in a glovebox filled with Ar of 99.999% purity for 4 months (called the milled and exposed LiH hereafter), and (iv) the powder without ball milling, but stored in a glovebox filled with Ar of 99.999% for 4 months (termed the purchased and exposed LiH hereafter).

The phase composition of the oxidized LiH powders as a function of the exposing time was calculated from the XRD patterns by the normalized-intensity-ratio (NIR) method. The NIR method uses the kinematics XRD theory to calculate the volume fraction of the jth crystalline phase ($X_j^{(V)}$) in a combination of n crystalline phases through the equation:

$$X_j^{(V)} = \frac{I_{jg} V_j^2 e^{2B_{jg}}}{K m_{jg} L P_{jg} F_{jg}^{\ 2}} \tag{7}$$

where I_{jg}, $e^{2B_{jg}}$, m_{jg}, LP_{jg}, and F_{jg} are the integrated intensity, the Debye−Waller temperature factor, the multiplicity, the Lorentz-polarization factor, and the structure factor of the gth Bragg reflection of the jth phase, respectively. The term V_j is the unit cell volume of the jth phase, whereas K is a constant that depends on both diffractometer and sample features. In practice, I_{jg} and V_j in eq 7 are obtained from the XRD data, whereas the rest of factors in eq 7 are readily calculated from the crystal structure of the jth phase, thus avoiding the use of internal or external standards. Consequently, the volume fraction of all phases in the specimen are calculated by formulating and solving a square system constituted by a set of eq 7. However, usually the constant K is not evaluated explicitly, and therefore, the magnitudes calculated directly from the resolution of the square system are the product $KX_j^{(V)}$. After knowing all $KX_j^{(V)}$, the corresponding $X_j^{(V)}$ are then calculated by imposing the normalization condition as follows:

$$X_j^{(V)} = \frac{KX_j^{(V)}}{\sum_{j=1}^{n} KX_j^{(V)}} \tag{8}$$

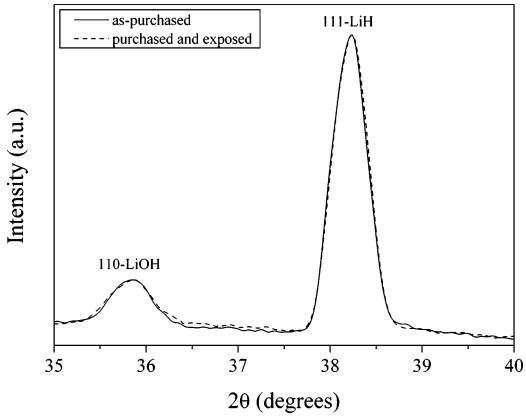

Figure 1. Experimental XRD patterns for the as-purchased LiH (solid line) and the purchased and exposed LiH (dashed line). For comparison, the two patterns have been normalized by imposing the same peak intensity for the 111 Bragg reflection of the LiH phase.

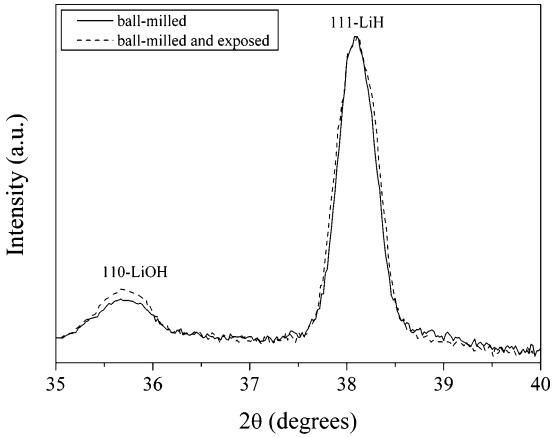

Figure 2. Experimental XRD patterns for the ball-milled LiH (solid line) and the milled and exposed LiH (dashed line). For comparison, the two patterns have been normalized by imposing the same peak intensity for the 111 Bragg reflection of the LiH phase.

In the present study, the terms I_{jg} and V_j for eq 7 were obtained, respectively, from the area and position of the CuK_α1 component of the Bragg reflections of the phases present, which were determined by analytical profile fitting assuming Voigt functions with CuK_α1 and CuK_α2 components for the modeling of the Bragg reflections and a first-order polynomial function for the modeling of the background; the fits were conducted iteratively by the Levenberg−Marquardt nonlineal least-squares algorithm. These areas directly yielded the integrated intensities, whereas these positions yielded V_j through the Bragg law coupled with the plane-spacing equations for the different crystal systems.

III. Results and Discussion

3.1. Stability of LiH Under a High-Purity Ar Atmosphere at Room Temperature. The experimental XRD patterns of the as-purchased LiH and the purchased LiH with a subsequent exposure to an argon atmosphere of 99.999% purity at room temperature for 4 months are shown in Figure 1. Note that the ratios of LiH/LiOH integrated intensities are identical for the LiH powder with and without 4-month exposure to the argon atmosphere. The phase composition calculated from eqs 7 and 8 for the as-purchased LiH is 94.1 vol % LiH + 5.9 vol % LiOH. The corresponding value for the purchased LiH with a subsequent exposure to an argon atmosphere for 4 months is 93.9 vol % LiH + 6.1 vol % LiOH. The minute difference between the two samples is within the experimental error (about 0.5 vol %), and thus it is concluded that there is no discernible difference in the phase composition between the two samples. This result indicates that there is no oxidation when the as-purchased LiH is stored at room temperature under an argon atmosphere of 99.999% purity with H_2O < 1 ppm, O_2 < 1 ppm, H_2 < 3 ppm, N_2 < 5 ppm, and THC < 0.5 ppm. The result also reveals that the as-purchased LiH contains 6.0 vol % LiOH.

Figure 2 shows the experimental XRD patterns of the as-milled LiH and the milled LiH with a subsequent exposure to an argon atmosphere of 99.999% purity at room temperature for 4 months. Note that the same phenomenon as the LiH without ball milling is found, that is, the ratio of LiH/LiOH integrated intensities are identical for the ball-milled LiH with and without 4-month exposure to an argon atmosphere. The phase composition for the as-milled LiH is found to be 94.0 vol % LiH + 6.0 vol % LiOH, and the corresponding value for the milled and exposed LiH is 93.7 vol % LiH + 6.3 vol % LiOH. Since the minute difference in the phase composition between the two samples is within the experimental error (about 0.5 vol %), it can be concluded that no oxidation takes place when the ball-milled LiH powder is exposed to an argon atmosphere of 99.999% purity for 4 months at room temperature.

Two additional conclusions can be made by comparing the LiH with and without ball milling. First, there is no oxidation during the ball milling process, indicating that the seal of the canister of the attritor is airtight, and there is no leaking of argon gas during ball milling. Second, the oxidation of LiH, if any, under a high-purity argon atmosphere is extremely slow at room temperature, regardless of the powder particle sizes. It is well-known that ball milling can reduce powder particle sizes dramatically, often from tens of micrometers to tenths of micrometers.[23,24] The measurement of the specific surface area (SSA) of the LiH powder with and without ball milling confirms this trend. Using the BET method, it is found that the as-purchased LiH has a SSA of 4.614 m^2/g, whereas the ball-milled LiH has a SSA of 13.104 m^2/g. Based on these SSA data and assuming that the particles are spherical, the equivalent particle radius can be calculated, and is found to be 0.79 μm for the as-received LiH and 0.28 μm for the ball milled LiH. Thus, the above data unambiguously show that both coarse and fine LiH particles are stable at room temperature under an argon atmosphere of 99.999% purity, as one would expect since argon is an inert gas.

3.2. Stability of LiH in Ambient Air at Room Temperature. Shown in Figure 3a and 3b are selected experimental XRD patterns of LiH with and without ball milling, collected in situ during the exposure to ambient air at room temperature. It can be seen that as the exposure time increases, the integrated intensities of LiOH peaks increase, which is accompanied by a continued decrease in the integrated intensities of LiH peaks. This is true for both milled and unmilled LiH powders, indicating that LiH is oxidized and the oxidation product is LiOH for both milled and unmilled powders.

The result from the quantitative phase composition analysis based on the XRD data is shown in Figure 4. As expected, the volume fraction of the oxidation product, LiOH, continues to increase, while the volume fraction of LiH decreases with the exposure time. Both the milled and unmilled LiH exhibit the same trend. However, the oxidation rate of the milled LiH is faster than that of the unmilled LiH, as shown in Figure 5.

There are several possible reaction routes that can lead to the formation of LiOH when LiH is exposed to air at room temperature. Thermodynamic calculations[25] indicate that all of the reactions 5, 6, and 9−11, listed below along with their

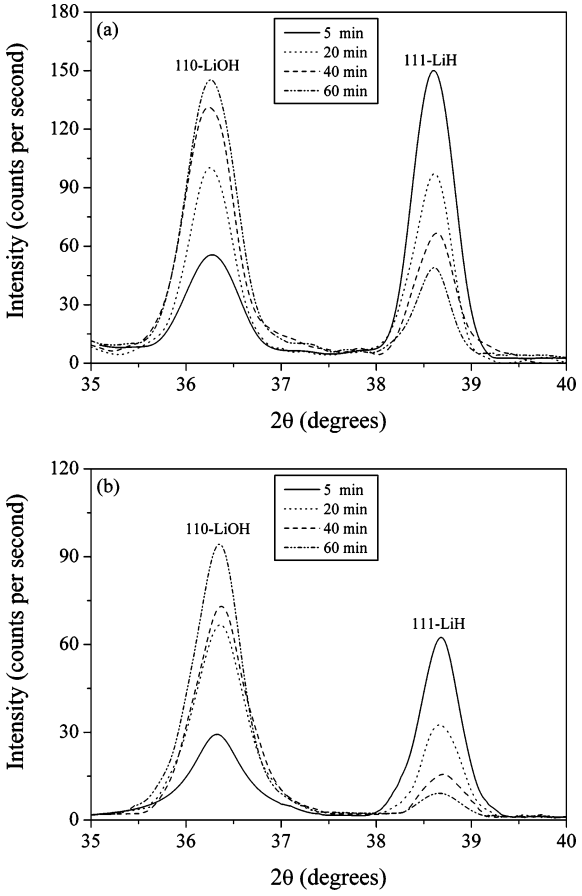

Figure 3. Experimentally measured XRD patterns of LiH exposing to ambient air at room temperature as a function of the exposure time: (a) without milling and (b) with milling for 3 h at 20 °C in Ar of 99.999% purity.

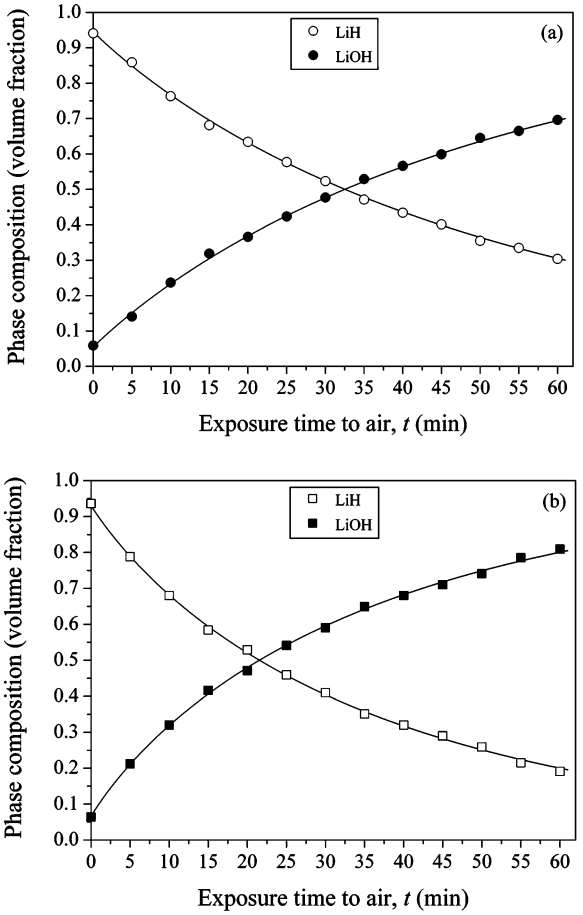

Figure 4. Volume fraction of the phases present in (a) the as-purchased LiH and (b) the ball-milled LiH as a function of the exposure time to ambient air at room temperature. The error bars are lower than the point size, and the solid curves are guides for the eyes.

corresponding standard Gibbs free-energy changes, are thermodynamically possible.

$$\mathrm{LiH} + {}^1/_2\,\mathrm{H_2O} = {}^1/_2\,\mathrm{Li_2O} + \mathrm{H_2} \qquad \Delta G = -93.98\ \mathrm{kJ/mol} \quad (5)$$

$$\mathrm{LiH} + \mathrm{H_2O} = \mathrm{LiOH} + \mathrm{H_2} \qquad \Delta G = -133.01\ \mathrm{kJ/mol} \quad (6)$$

$$\mathrm{LiH} + {}^1/_2\,\mathrm{O_2} = \mathrm{LiOH} \qquad \Delta G = -370.24\ \mathrm{kJ/mol} \quad (9)$$

$$\mathrm{LiH} + {}^1/_4\,\mathrm{O_2} = {}^1/_2\,\mathrm{Li_2O} + {}^1/_2\,\mathrm{H_2} \qquad \Delta G = -212.59\ \mathrm{kJ/mol} \quad (10)$$

$$\mathrm{Li_2O} + \mathrm{H_2O} = 2\ \mathrm{LiOH} \qquad \Delta G = -78.06\ \mathrm{kJ/mol} \quad (11)$$

Both reactions 6 and 9 lead to the formation of LiOH directly, while reactions 5 and 10 produce Li_2O first which subsequently reacts with H_2O to form LiOH. Since in the entire exposure period there is not any trace of Li_2O, it can be concluded that either reactions 5 and 10 do not occur at all, or reaction 11 proceeds extremely fast so that Li_2O disappears as soon as it forms from reactions 5 and 10. The latter is very unlikely because a previous study[26] has shown that the conversion between Li_2O and LiOH as defined by eq 11 can be easily followed using elastic proton backscattering in a matter of several hours, indicating that reaction 11 is sluggish. Thus, the oxidation of LiH in ambient air with ~27% relative humidity must proceed with reaction 6, 9, or both.

Both reactions 6 and 9 are thermodynamically possible and have indeed occurred. As will be shown in Section 3.3, LiH

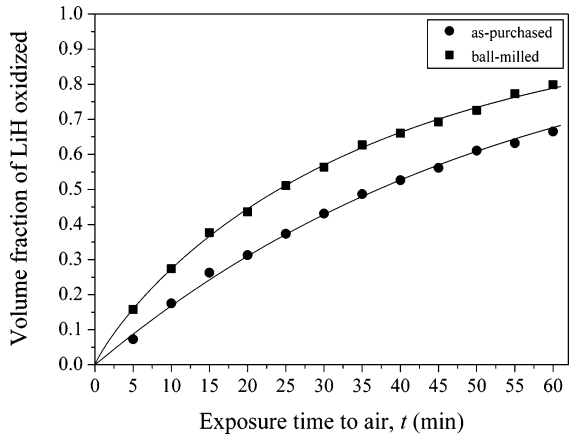

Figure 5. Comparison in the oxidation rate under ambient air at room temperature between the LiH powders with and without ball-milling. The error bars are lower than the point size. The solid lines are generated using the Johnson−Mehl−Avrami models (to be discussed in the text).

reacts with H_2O as well as O_2 even when LiH is exposed to an argon atmosphere containing 515 ppm O_2 (i.e., 0.0515 vol %) and 5692 ppm H_2O (0.569 vol %) at room temperature. For the ambient air studied here, the concentrations of O_2 and H_2O are 20.9 and 0.81 vol %, respectively, both of which are higher than those of O_2 and H_2O in the argon atmosphere to be discussed in Section 3.3. Thus, it is reasonable to deduce that LiH reacts with both O_2 and H_2O in ambient air with a 27% relative humidity at 25 °C to form LiOH, as indicated by reactions 6 and 9. In what follows, the reaction kinetics will be

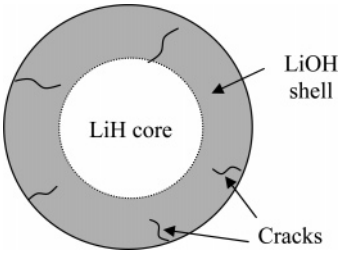

Figure 6. Schematic of the oxidation of LiH particles in ambient air.

discussed for both reactions 6 and 9. However, reaction 6 will be analyzed first, and the result will be applied to reaction 9.

Based on the formula of reaction 6, it can be stated that the rate control mechanism for oxidation of LiH in air can be (i) evaporation of the H_2 gas, (ii) concentration of the reactant, LiH, (iii) diffusion of oxygen, hydrogen, or water through the LiOH layer, (iv) movement of the LiH/LiOH phase boundary, or (v) nucleation and growth of LiOH. It is well established that if the oxidation is controlled by evaporation of the gaseous product, the volume fraction of the oxidation product will follow a linear-rate law[27]

$$f = k_1 t \tag{12}$$

where f stands for the volume fraction of the oxidation product, k_1 is a rate constant, and t is the time during an isothermal reaction. If the oxidation rate is controlled by the concentration of the reactant, then the functional dependency of f on t is given by the following equation[28]

$$f = 1 - \left[\frac{n-1}{k_2 {m_0}^{n-1} t}\right]^{1/n-1} \tag{13}$$

where n is the order of reaction, m_0 is the initial mass of the reactant, and k_2 is a rate constant. If the reaction is a first order reaction, the volume fraction of the reaction product can then be expressed in a relatively simple form[28]

$$f = 1 - \exp(-k_2 t) \tag{14}$$

If the oxidation product, LiOH, forms a dense layer on the surface of LiH, the oxidation rate will be controlled by the diffusion of water through the LiOH layer, or by the diffusion of oxygen because the diffusion rate of hydrogen is typically much faster than that of oxygen if water dissociates into oxygen and hydrogen.[29] A parabolic-rate law will be observed for such a diffusion-controlled reaction.[27] Given that the LiH in this study is in a particle form, it is reasonable to assume that the oxidation of LiH would occur via growth of a shell of LiOH into the interior of a LiH particle if the oxidation of LiH is diffusion-controlled (see Figure 6). It is easy to show that with such a LiOH-growth mechanism, the volume fraction of LiOH as a function of the reaction time is

$$f = 1 - \left[1 - \frac{{k_3}^{1/2}}{R} t^{1/2}\right]^3 \tag{15}$$

where R is the original average radius of LiH particles and k_3 is a rate constant. However, if the oxidation of LiH is controlled by the movement of the LiH/LiOH phase boundary, the volume fraction of LiOH as a function of time would have the following form:[15]

$$f = 1 - \left[1 - \frac{k_4}{R} t\right]^3 \tag{16}$$

where k_4 is a rate constant. Finally, if the oxidation of LiH is controlled by nucleation and subsequent growth of LiOH, the volume fraction of LiOH as a function of time can then be expressed by the well-known Johnson−Mehl−Avrami (JMA) equation[30]

$$f = 1 - \exp(-k_5 t^m) \tag{17}$$

where m is the mechanism constant which varies from 1 to 4, depending on the detail of nucleation and growth of LiOH, and k_5 is the rate constant affected by nucleation and growth mechanisms as well.

To find out the rate-controlling mechanism, eqs 12, 13, 15, 16 and 17 should be fitted to the experimental data obtained from the quantitative XRD analysis, and the degree of discrepancy between the theoretical prediction and the experimental data be quantified in terms of the reduced chi-squares (χ_r^2). Curve fitting through the least-squares method results in two linear relationships from each of these attempts, one for the unmilled LiH and the other for the milled LiH. Once the parameters for all of the five possible rate-controlling mechanisms are determined, comparisons between these possible rate-controlling mechanisms and the experimental data can be performed by plotting the predictions from various rate-controlling mechanisms and the experimental data in a single f-versus-t chart. Of course, the most likely rate-controlling mechanism is the one yielding the lowest χ_r^2. Shown in Figures 7a and b are such plots for the unmilled LiH and milled LiH, respectively. It can be seen that the nucleation and growth mechanism, i.e., eq 17, fits the experimental data best ($\chi_r^2 = 0.00049$ for the unmilled LiH and $\chi_r^2 = 0.0001$ for the milled LiH), followed by the movement of the LiH/LiOH phase boundary mechanism ($\chi_r^2 = 0.0011$ for the unmilled LiH and $\chi_r^2 = 0.0042$ for the milled LiH). Thus, it can be concluded that the oxidation of LiH in air at room temperature is not controlled by evaporation of H_2 ($\chi_r^2 = 0.00711$ for the unmilled LiH and $\chi_r^2 = 0.02214$ for the milled LiH), the higher order reaction of the concentration of LiH in the powder ($\chi_r^2 = 0.00952$ for the unmilled LiH and $\chi_r^2 = 0.00815$ for the milled LiH), and diffusion of oxygen or hydrogen atoms through the LiOH layer ($\chi_r^2 = 0.02518$ for the unmilled LiH and $\chi_r^2 = 0.01129$ for the milled LiH). Instead, the oxidation rate of LiH in air is controlled by the nucleation and growth of LiOH or by the movement of the LiH/LiOH phase boundary. Note that the difference between these two mechanisms is, in fact, very small, as discussed below.

The JMA equation describing the mechanism of the nucleation and growth of LiOH, obtained through the curve fitting for the oxidation of the as-purchased LiH in air at room temperature, is

$$f = 1 - \exp(-0.018 t^{1.01}) \tag{18}$$

and it becomes

$$f = 1 - \exp(-0.028 t^{1.01}) \tag{19}$$

for the ball-milled LiH. The equations describing the mechanism of the LiH/LiOH phase boundary movement, obtained via curve fitting, are

$$f = 1 - (1 - 0.0056t)^3 \tag{20}$$

and

$$f = 1 - (1 - 0.0080t)^3 \tag{21}$$

for the as-purchased and ball-milled LiH, respectively.

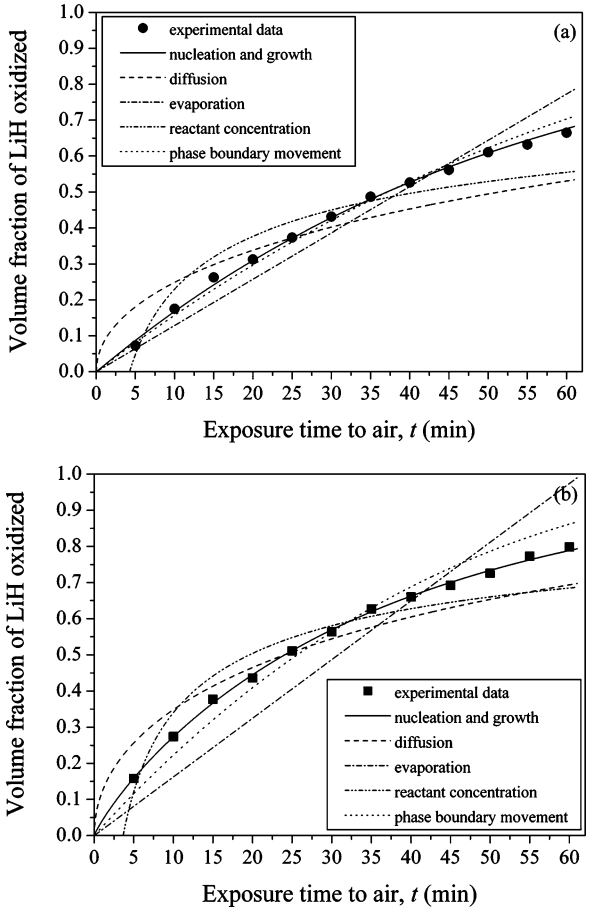

Figure 7. Comparisons among all of the possible rate-controlling mechanisms using the least-squares prediction equations and the volume fraction of the experimentally determined LiOH as a function of the oxidizing time for (a) the as-purchased LiH and (b) the ball-milled LiH in air at room temperature. The error bars for experimental data are lower than the point size. See the text for details.

It is well established that, for solid-state transformations with one-directional growth, the *m* constant in the JMA equation will be between 1 and 2.[30] Furthermore, when $m = 1$, the reaction product nucleates at the beginning of the reaction, and the subsequent transformation is controlled by the one-directional growth of the reaction product.[30] Based on this established mechanism and the *m* constant in eqs 18 and 19, it can be stated that the oxidation of the as-purchased and ball-milled LiH in air at room temperature proceeds by the formation of all the LiOH nuclei on the surface of the LiH particles at the beginning of the reaction, followed by the subsequent growth of these nuclei into the interiors of the LiH particles, as shown schematically in Figure 6.

The difference between eqs 18 and 20 is that eq 18 takes into the consideration of nucleation events, whereas eq 20 assumes that nucleation takes place instantaneously and the entire transformation process is controlled by the growth of LiOH into the LiH particle only. Since eq 18 fits the experimental data better than eq 20 as shown in Figure 7a, it is reasonable to conclude that the nucleation event accounts for a noticeable period of time during the oxidation of LiH in air at room temperature. The same conclusion can be made for the milled LiH powder by comparing eqs 19 and 21, as supported by the observation of Figure 7b.

Note that since the *m* constants in eqs 18 and 19 are the same for the uilled and milled LiH powders, it can be concluded that the oxidation mechanisms for these two powders are identical. However, the milled LiH powder oxidizes faster because it has a larger k_5 (see eq 17) or k_4/R (see eq 16) than the unmilled LiH powder, i.e., 0.028 vs 0.018 in eqs 19 and 18, and 0.0080 vs 0.0056 in eqs 21 and 20, respectively. The faster oxidation rate of the milled LiH is due to its finer particle size and larger surface area.

The conclusions obtained above are consistent with the SEM observation. Shown in Figure 8 are SEM images of the typical surfaces of (i) the as-purchased LiH particles with an exposure to air at room temperature in less than 1 min before being coated with a thin layer of Au and (ii) the purchased and exposed LiH particles which have been intentionally exposed to air at room temperature for 10 min before being coated with a thin layer of Au. It is very clear that the density of microcracks on the surface of the oxidized LiH particle increases from less than 1-min exposure to 10-min exposure. The increase in the microcrack density is consistent with the measurement of the specific surface area, which has the experimental error of ± 0.35 m^2/g and shows that the SSA of LiH particles increases from 4.61 m^2/g to 6.56 m^2/g after exposure to air for 10 min at room temperature. This increased density of microcracks eliminates the dependence of the continued oxidation of LiH particles on the diffusion of oxygen or hydrogen through the LiOH surface layer. As a result, the oxidation of LiH is controlled by the formation of LiOH nuclei and the subsequent movement of the LiH/LiOH phase boundary.

Finally, it should be pointed out that the conclusions obtained for reaction 6 are also applicable to reaction 9. This is true because the formation of LiOH from reaction 9 will be on the surface of LiH particles. As a result, the subsequent oxidation will also rely on the movement of the LiH/LiOH phase boundary.

3.3. Stability of LiH Under an Ar Atmosphere with O_2 and H_2O Impurities. The stability of LiH under an argon atmosphere with some impurities of O_2, H_2O, N_2, H_2 and NH_3 was evaluated using a TGA apparatus in conjunction with a RGA for the outlet gas analysis. Shown in Figure 9 is the outlet gas composition from the TGA apparatus with an empty pan (i.e., a blank sample) and a flowing argon atmosphere of 99.999% purity. It is clear that immediately after the close of the TGA chamber (the zero point of time), all of the gaseous species (N_2, O_2, H_2O, and H_2) except Ar exhibit a general trend of decreasing concentrations with time. Ar is the only exception to this rule. It increases with time initially and in less than 10 min the argon concentration has reached its steady-state value. In contrast, the concentrations of all other species decrease continuously even after 180 min at which the experiment is stopped. As expected, the onset of heating at 90 min and the subsequent heating do not impose any interference to the variation of the gaseous composition with time. All of these phenomena can be explained based on the fact that ambient air in the TGA chamber is gradually replaced by the flowing argon. The quantitative analysis indicates that the concentrations of H_2O, O_2, H_2, and N_2, in the outlet gas at 90 min are 5692, 515, 585, and 88 ppm, respectively, and the corresponding values for these gaseous species at 180 min are 4541, 443, 530, and 72 ppm.

Figure 10 shows the weight change of the as-purchased LiH as a function of time after the heating starts at 90-min of holding. There are several interesting features in this figure. First, LiH is oxidized during 90-min of holding at room temperature. This oxidation has resulted in a 1% increase in weight and is due to the presence of O_2 and H_2O impurities in the TGA chamber (see Figure 9 and additional discussion below). The 1% increase

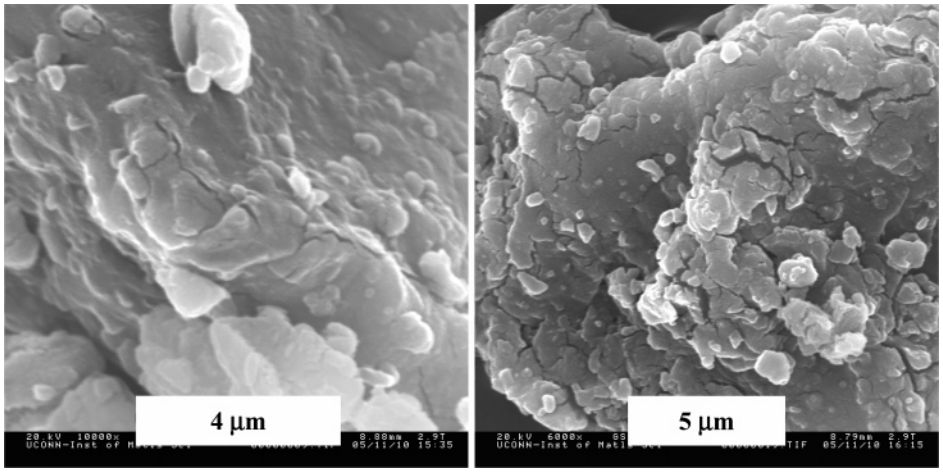

Figure 8. SEM images of the as-purchased LiH with a subsequent exposure to air at room temperature for (a) less than 1 min and (b) about 11 min.

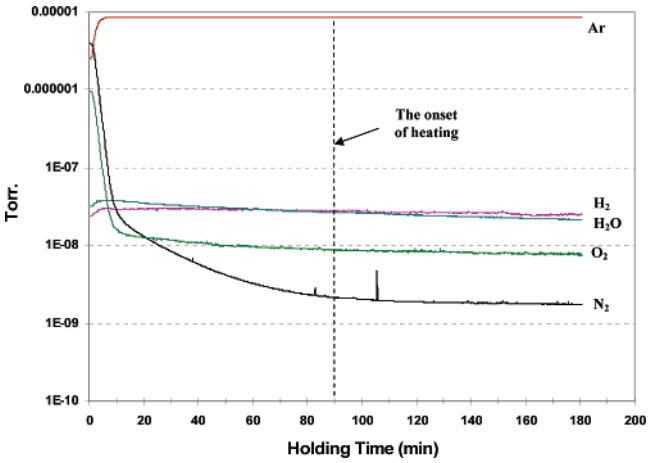

Figure 9. The composition profile of the outlet gas for a blank sample in the TGA apparatus as a function of the holding time. A flowing argon atmosphere of 99.999% purity was provided immediately after the close of the TGA chamber at 25 °C. The time at which the TGA chamber is closed is taken as the zero point, and at 90 min the TGA chamber is heated at a heating rate of 5 °C/min.

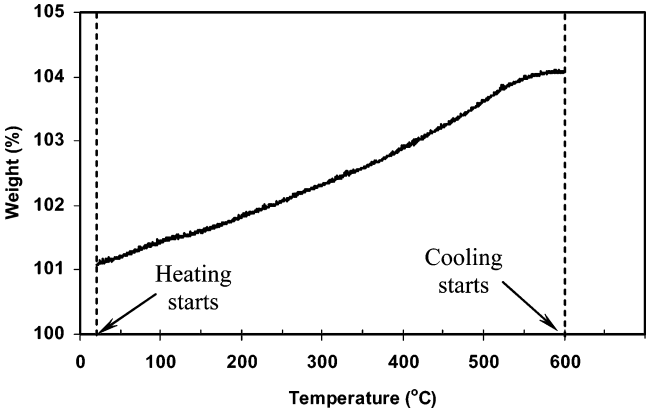

Figure 10. TGA curve of the as-purchased LiH in a flowing argon atmosphere with a constant heating rate of 5 °C/min. The sample has been held in the TGA chamber with a flowing argon of 99.999% purity for 90 min at room temperature before the heating starts, and the cooling is initiated when temperature reaches 600 °C.

in weight would represent oxidation of 0.41 vol % LiH in the system if the oxidation occurs via either reaction 6 or 9. Second, the weight gain (i.e., another 3% increase) is observed in the entire heating period (from 25 to 600 °C), indicating the continued oxidation of LiH during heating. Last, the slope of the weight gain appears to increase at ∼390 °C, suggesting an increase in the oxidation rate above 390 °C.

Shown in Figure 11 is the outlet gas composition as a function of temperature for the as-purchased LiH in the TGA chamber with an identical experimental condition as that in Figure 10. The important features to be noted from this figure are as follows. (i) The hydrogen concentration exhibits obvious increases at ∼40 °C, suggesting the increased oxidation rate right after the increase in temperature. (ii) Two hydrogen concentration peaks are observed, one at 130 °C and the other at 600 °C after which the TGA chamber starts to cool. (iii) The oxygen concentration exhibits a precipitous decrease at ∼55 °C, and continues to decrease as temperature increases. However, the oxygen concentration starts to increase when the cooling is initiated after reaching 600 °C. (iv) Heating does not affect the gradual decrease in the N_2 concentration. The latter is caused by the gradual replacement of ambient air by the flowing argon. (v) The concentration of H_2O exhibits a general trend of decrease as temperature and time increase. However, two peaks are superimposed on this general trend with one appearing at ∼150 °C and the other at 600 °C.

The composition change as a function of temperature and time observed in Figure 11 provides direct evidence for deducing the oxidation mechanism of LiH in a flowing argon with less than 5692 ppm H_2O, 515 ppm O_2, 585 ppm H_2, and 88 ppm N_2 impurities. Based on the phenomena observed in Figure 11 and the comparison with eqs 5, 6, 9, and 10, the following conclusions can be made. First, the weight gain observed in Figure 10 is not induced by N_2 because N_2 exhibits a continuous and gradual decrease with time for the entire holding and heating period. Second, the weight gain from ∼55 to 600 °C is caused by the O_2 impurity. Furthermore, the oxidation of LiH proceeds with reaction 10 because this reaction results in a decrease in O_2 and an increase in H_2 simultaneously. This is exactly what is observed in Figure 11. Third, reactions 5 and 6, which also produce H_2, play a minimal role in the oxidation of LiH from ∼55 to 600 °C under the condition investigated. This is supported by the fact that the H_2O concentration in the outlet gas continues to decrease at the cooling stage after 600 °C, whereas the O_2 concentration increases, instead, at the cooling stage. The increased O_2 concentration at the cooling stage [Figure 11c] indicates a decrease in the oxidation rate of LiH and thus less consumption of O_2 in the flowing argon as the temperature decreases. In contrast, the continued decrease in the H_2O concentration after cooling from 600 °C [Figure 11b] can only be explained by the continued replacement of the

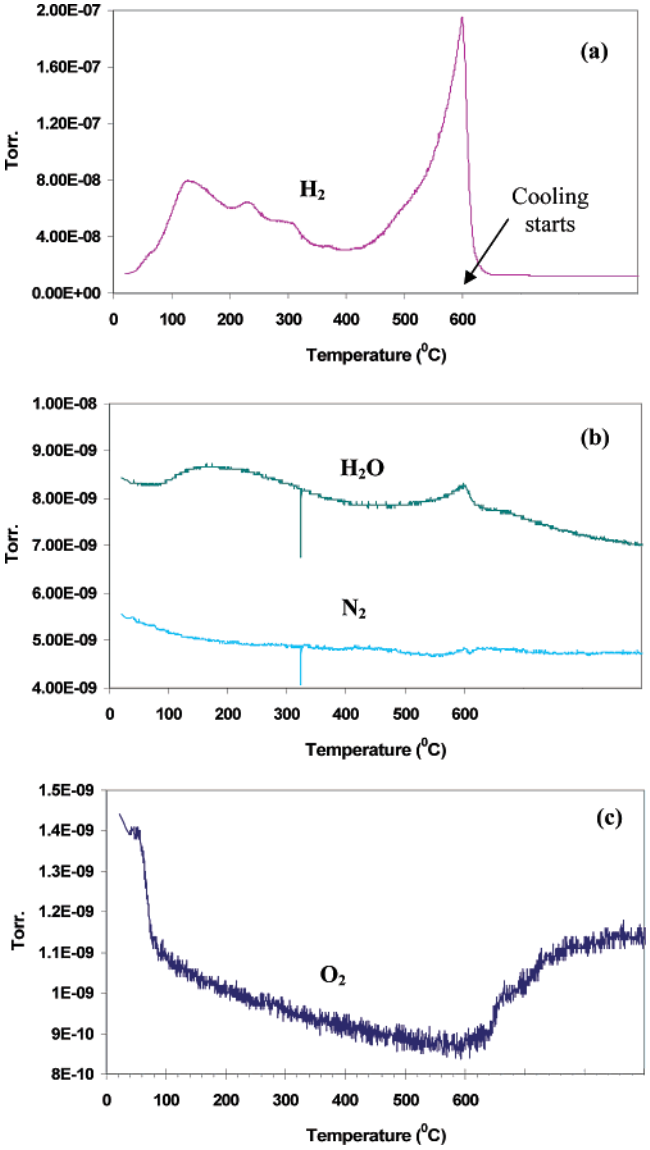

Figure 11. The variation of the outlet gas composition as a function of temperature for the as-purchased LiH sample in the TGA chamber with the experimental condition identical to that in Figure 10: (a) H_2, (b) H_2O and N_2, and (c) O_2. Note that the cooling is initiated at 600 °C. Thus, the composition changes after the onset of cooling should be taken as the variation as a function of time.

residual H_2O from ambient air by the flowing argon. Therefore, it can be concluded that H_2O plays a minimum role in the oxidation of LiH in the heating stage from ~55 to 600 °C. Fourth, the two H_2O peaks are generated via the following reaction

$$H_2 + {}^1/_2\, O_2 = H_2O \qquad (22)$$

This conclusion is supported by the fact that the two H_2O peaks appear at the same time as the two H_2 peaks, that is, the increased H_2 concentration drives reaction 22 toward the formation of H_2O. Fifth, the two H_2 peaks are believed to be related to the change in the oxidation rate of LiH with temperature and possibly with the formation of a Li_2O shell on the surface of the LiH particle. The exact mechanism(s) for this phenomenon are not investigated in this study. However, one possible explanation would be the formation of the Li_2O shell which leads to a reduction in the oxidation rate of LiH at temperatures higher than 135 °C but below 400 °C. The subsequent cracking of this Li_2O shell results in a substantial increase in the oxidation rate at temperatures higher than 400 °C. This proposition needs to be verified in a future study.

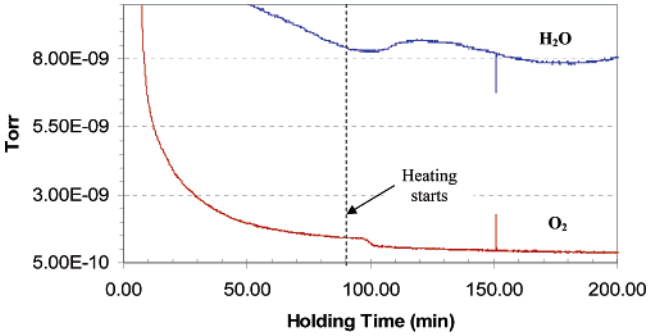

Figure 12. The variation of H_2O and O_2 concentrations in the outlet gas as a function of the holding time near 90-min of holding for the as-purchased LiH sample in the TGA chamber. The experimental condition is identical to that shown in Figures 10 and 11.

Finally, it is worthwhile to examine the oxidation mechanism of LiH at room temperature under the flowing argon atmosphere with H_2O and O_2 impurities. This can be done by studying how the concentrations of H_2O and O_2 in the outlet gas vary with the holding time for a LiH sample before heating starts at 90-min of holding. Shown in Figure 12 are details of H_2O and O_2 concentrations as a function of the holding time near 90-min of holding for a LiH sample in the TGA chamber. A comparison with the blank sample (Figure 9) reveals that at 90-min of holding the concentration of H_2O in the outlet gas with a LiH sample in the TGA chamber is lower than that of H_2O without a LiH sample by a factor of 0.1, indicating that some H_2O in the TGA chamber has reacted with the LiH sample. Similarly, the concentration of O_2 in the outlet gas with a LiH sample in the TGA chamber is lower than that of O_2 without a LiH sample by a factor of 0.2, indicating that some O_2 in the TGA chamber has also reacted with the LiH sample.

The fact that the outlet gas has lower concentrations of O_2 and H_2O when the TGA chamber contains a LiH sample provides clear evidence for the reaction of LiH with the O_2 and H_2O impurities in the flowing argon at room temperature. Such reactions are most likely due to reactions 6 and 9. This conclusion is reached based on the following argument. First, reaction 5 is unlikely because the H_2O impurity in the present study (5692 ppm) is much higher than what is needed to react with one surface layer of LiH. Reaction 5 only occurs when the amount of water is only sufficient to react with one surface layer of LiH.[13] Second, reaction 10 has been identified to occur at temperatures higher than ~55 °C. Below 55 °C different oxidation mechanisms are present because a sudden increase in the oxygen consumption takes place at ~55 °C (Figure 11c). Thus, reactions 6 and 9 are the remaining reactions that can account for the decrease in the O_2 and H_2O concentrations observed at room temperature. Finally, the conclusion that reactions 6 and 9 are operational at room temperature is consistent with the formation of only LiOH observed when LiH is exposed to ambient air, as discussed in Section 3.2. It is also in good agreement with a previous study[31] which shows that at a given oxidation environment, LiOH is preferentially formed at lower temperatures, while Li_2O is formed predominately at higher temperatures.

IV. Summary and Conclusions

The stability of LiH in high purity argon, argon with some O_2 and H_2O impurities, and ambient air has been investigated.

Effects of ball milling on the LiH stability have also been examined. Based on this study, the following conclusions can be offered.

1. No oxidation of LiH occurs at room temperature under an argon atmosphere of 99.999% purity with H_2O < 1 ppm, O_2 < 1 ppm, H_2 < 3 ppm, N_2 < 5 ppm, and THC < 0.5 ppm.

2. This conclusion remains true even after LiH particles have been subjected to ball milling with an increase in the specific surface area to 13.1 m^2/g and a reduction in the equivalent particle size to 0.56 μm in diameter.

3. The oxidation product of LiH in ambient air with a relative humidity of 27% at room temperature is LiOH.

4. The oxidation kinetics of LiH in ambient air at room temperature is controlled by nucleation and growth processes. LiOH nucleates on the surface of the LiH particle at the beginning of the reaction, and the subsequent reaction is controlled by the one-directional growth of LiOH into the LiH core.

5. The oxidation kinetics of LiH in ambient air at room temperature can be described very well by the Johnson−Mehl−Avrami equation:

$$f = 1 - \exp(-0.018t^{1.01}) \text{ for the unmilled LiH}$$

$$f = 1 - \exp(-0.028t^{1.01}) \text{ for the ball-milled LiH}$$

The ball-milled LiH has a faster oxidation rate than the unmilled LiH because the ball-milled LiH has a larger specific surface area and finer particle size.

Oxidation of LiH occurs under an argon atmosphere containing 5692 ppm H_2O, 515 ppm O_2, 585 ppm H_2, 88 ppm N_2, and 1.3 ppm NH_3. At temperatures ranging from ~55 to 600 °C, oxidation of LiH proceeds via the following equation:

$$\mathrm{LiH} + {}^1/_4\,\mathrm{O_2} = {}^1/_2\,\mathrm{Li_2O} + {}^1/_2\,\mathrm{H_2}$$

7. At room temperature, oxidation of LiH in ambient air and in an argon atmosphere containing 5692 ppm H_2O, 515 ppm O_2, 585 ppm H_2, 88 ppm N_2, and 1.3 ppm NH_3 is most likely due to the following two reactions:

$$\mathrm{LiH} + \mathrm{H_2O} = \mathrm{LiOH} + \mathrm{H_2}$$

$$\mathrm{LiH} + {}^1/_2\,\mathrm{O_2} = \mathrm{LiOH}$$

Acknowledgment. This work was supported under the U.S. Department of Energy (DOE) contract no. DE-FC36-05GO15008. The vision and support of Dr. Carole Read, DOE Technology Manager, is greatly appreciated.

References and Notes

(1) Chen, P.; Xiong, Z.; Luo, J. Z.; Lin, J. Y.; Tan, K. L. Interaction of hydrogen with metal nitrides and imides. *Nature* **2002**, *420*, 302.

(2) Chen, P.; Xiong, Z.; Luo, J. Z.; Lin, J. Y.; Tan, K. L. Interaction between lithium amide and lithium hydride. *J. Phys. Chem. B* **2003**, *107*, 10967.

(3) Hu, Y. H.; Ruckenstein, E. H_2 storage in Li_3N. Temperature-programmed hydrogenation and dehydrogenation. *Ind. Eng. Chem. Res.* **2003**, *42*, 5135.

(4) Hu, Y. H.; Ruckenstein, E. Ultrafast reaction between LiH and NH_3 during H_2 storage in Li_3N. *J. Phys. Chem. A* **2003**, *107*, 9737.

(5) Ichikawa, T.; Hanada, N.; Isobe, S.; Leng, H.; Fujii, H. Mechanism of novel reaction from $LiNH_2$ and LiH to Li_2NH and H_2 as a promising hydrogen storage system. *J. Phys. Chem. B* **2004**, *108*, 7887.

(6) Ichikawa, T.; Isobe, S.; Hanada, N.; Fujii, H. Lithium nitride for reversible hydrogen storage. *J. Alloys Compd.* **2004**, *365*, 271.

(7) Orimo, S.; Nakamori, Y.; Kitahara, G.; Miwa, K.; Ohba, N.; Noritake, T.; Towata, S. Destablization and enhanced dehydriding reaction of $LiNH_2$: an electronic structure viewpoint. *Appl. Phys. A* **2004**, *79*, 1765.

(8) Ichikawa, T.; Hanada, N.; Isobe, S.; Leng, H.; Fujii, H. Composite materials based on light elements for hydrogen storage. *Mater. Trans.* **2005**, *46*, 1.

(9) Kojima, Y.; Kawai, Y. IR characterization of lithium imide and amide. *J. Alloys Compd.* **2005**, *395*, 236.

(10) Hu, Y. H.; Ruckenstein, E. Highly effective Li_2O/Li_3N with ultrafast kinetics for H2 storage. *Ind. Eng. Chem. Res.* **2004**, *43*, 2464.

(11) Ordaz, G.; Petrovic, J.; Read, C.; Satyapal, S. Hydrogen storage. In CD of the *2005 Annual DOE Hydrogen Program Review Meeting*, Washington, DC, May 23−26, 2005; U.S. Department of Energy: Washington, DC, 2005.

(12) Holcombe, C. H. Retardation of the reaction of lithium hydride with water vapor. In *USAEC Report, Union Carbide Corp., Y-12 Plant, Y-1835/XAB;* USAEC: Aberdeen Proving Ground, MD, 1972.

(13) Machin, W. D.; Tompkins, F. C. Kinetics of the reaction of water vapor with crystalline lithium hydride. *Trans. Faraday Soc.* **1966**, *62*, 2205.

(14) Holcombe, C. E.; Powell, G. L. Some observations on the reaction layer of LiOH on LiH. *J. Nucl. Mater.* **1973**, *47*, 121.

(15) Dinh, L. N.; Cecala, C. M.; Leckey, J. H.; Balooch, M. The effects of moisture on LiD single crystals studied by temperature-programmed decomposition. *J. Nucl. Mater.* **2001**, *295*, 193.

(16) Gross, K. J.; Chartouni, D.; Leroy, E.; Züttel, A.; Schlapbach, L. Mechanically milled Mg composites for hydrogen storage: the relationship between morphology and kinetics. *J. Alloys Compd.* **1998**, *269*, 259.

(17) Liang, G.; Boily, S.; Huot, J.; Van Neste, A.; Schulz, R. Hydrogen absorption properties of a mechanically milled Mg-50 wt % $LaNi_5$ composite. *J. Alloys Compd.* **1998**, *268*, 302.

(18) Zaluski, L.; Zaluska, A.; Strom-Olsen, J. O. Hydrogen absorption in nanocrystalline Mg_2Ni formed by mechanical alloying. *J. Alloys Compd.* **1995**, *217*, 245.

(19) Orimo, S.; Fujii, H.; Ikeda, K. Notable hydriding properties of a nanostructured composite material of the Mg_2Ni−H system synthesized by reactive mechanical grinding. *Acta Mater.* **1997**, *45*, 331.

(20) Reule, H.; Hirscher, M.; Weiβhardt, A.; Kronmuller, H. Hydrogen desorption properties of mechanically alloyed MgH_2 composite materials. *J. Alloys Compd.* **2000**, *305*, 246.

(21) Yang, Z.-G.; Shaw, L. Synthesis of nanocrystalline SiC at ambient temperature through high energy reaction milling. *Nanostruct. Mater.* **1996**, *7*, 873.

(22) Brunauer, S.; Emmett, P. H.; Teller, E. Adsorption of gases in multimolecular layers. *J. Am. Chem. Soc.* **1938**, *60*, 309.

(23) Yang, Z.-G.; Ren, R.-M.; Shaw, L. Evolution of microstructures and nitrogen sorption during high energy milling of Si in ammonia. *J. Am. Ceram. Soc.* **2000**, *83*, 1897.

(24) Ren, R.-M.; Yang, Z.-G.; Shaw, L. Polymorphic transformation and powder characteristics of TiO_2 during high energy milling. *J. Mater. Sci.* **2000**, *35*, 6015.

(25) Barin, I.; Knacke, O.; Kubaschewski, O. Thermochemical properties of inorganic substances. Spinger-Verlag: Berlin, Germany, 1977.

(26) Myers, S. M. Ion-backscattering study of LiOH-to-Li_2O conversion on a LiH substrate. *J. Appl. Phys.* **1974**, *45*, 4320.

(27) *Oxidation and corrosion of intermetallic alloys;* Welsch, G., Desai, P. D., Eds.; Purdue Research Foundation: West Lafayette, Indiana, 1996.

(28) Speyer, R. F. Thermal analysis of materials. Marcel Dekker: New York, 1994.

(29) *Diffusion in solid metals and alloys;* Mehrer, H., Ed.; Springer-Verlag: New York, 1990; Vol 26.

(30) Dinh, L. N.; McLean, W. II; Schildbach, M. A.; LeMay, J. D.; Siekhaus, W. J.; Balooch, M. The nature and effects of the thermal stability of lithium hydroxide. *J. Nucl. Mater.* **2003**, *317*, 175.

(31) Christian, J. W. *The theory of transformations in metals and alloys: Part I;* Pergamon: Oxford, UK, 2002.